International Journal for Housing Science and Its Applications
Publish August 6, 2025. Volume 46, Issue 3 Pages 7706-7719

https://doi.org/10.70517/ijhsa463661

Automatic Detection and Performance Evaluation of Low-Orbit Satellite Signal Interference Based on Deep Belief Networks

Jieliang Zheng[1], Fenghua Xu[1], Yukun Zhu[1], Jian Zhou[1], Qiang Lv[2,*], Rui Guo[3] and Yu Chen[4]
[1] School of Computer Science and Engineering (School of Cyber Security), University of Electronic Science and Technology of China, Chengdu, Sichuan, 611731, China
[2] Beijing Guodiangaoke Co., Ltd., Beijing, 100095, China
[3] School of Information and Communication Engineering, University of Electronic Science and Technology of China, Chengdu, Sichuan, 611731, China
[4] Laboratory of Space Prevention, Control and Cyber Security, Qingdao Research Institute, Sichuan University, Qingdao, Shandong, 266000, China
Corresponding authors: (e-mail: lvqiang1980aa@163.com).

Abstract With the popularization of low-orbit satellite communication system, the impact of various types of interference signals on the quality of satellite communication has become increasingly serious. In this paper, for the automatic detection of various types of interference signals in low-orbit satellite communication system, an automatic interference signal detection method based on improved depth belief network is proposed. The study firstly establishes seven typical interference signal models, including single-tone interference, multi-tone interference, narrowband noise interference, broadband noise interference, comb spectrum interference, broadband linear sweep interference and impulse interference; and then extracts the signal characteristics from both time and frequency domains, focusing on the analysis of three characteristic parameters: 3dB bandwidth of normalized spectrum, peak-to-average ratio of the frequency domain, and moment skewness of the frequency domain; Then an improved deep belief network model introducing radial basis function activation function, combining -step contrast dispersion (CD)- and adaptive moment estimation algorithms is constructed to realize accurate classification and detection of interference signals. The experimental results show that the proposed method has good recognition effect in the range of dry noise ratio from -6dB to 13dB, and the AUC values for the seven kinds of interference signals as unknown signals are more than 0.7, among which the best detection effect is achieved for the comb spectral interference, with an AUC value of 0.806. The method has a false alarm probability of only 0.3 when the detection probability of the unknown interference is 0.8, which verifies the improvement of the depth belief network effectiveness and accuracy in the automatic detection of low-orbit satellite signal interference.

Index Terms Low-orbit satellite communication, interference signal detection, deep belief network, feature extraction, unknown interference detection, adaptive moment estimation

I. Introduction

With the development of satellite communication business, low orbit satellite communication has become a development hotspot in the field of space-based information system [1], [2]. Low-orbit satellites are located at the perigee of the Earth's orbit, so the distance between them and the ground is closer and the communication signal transmission speed is faster [3], [4]. In contrast, traditional terrestrial communication equipment is limited by factors such as geographic location and weather, and is susceptible to interference and cannot provide global communication services [5], [6]. Low-orbit satellite communication, on the other hand, can make up for these shortcomings by establishing a satellite network [7].

However, due to the high speed of LEO satellites orbiting the Earth, the frequency changes during signal transmission [8]. This phenomenon is caused by the Doppler effect, which directly affects the quality of satellite communications. When the satellite is close to the ground receiving end, the signal frequency is compressed and elevated, and when the satellite is far away the frequency is stretched and reduced [9], [10]. This frequency shift causes sound distortion in voice calls, similar to the change in pitch of a train whistle from far away to near [11]. Inter-symbol interference is triggered during data transmission, with a significant increase in the BER at the receiving end, and the navigation and positioning system is more significantly affected, with pseudo-range measurement errors of up to tens of meters generated by high-speed satellite movement [12]-[14]. In addition, satellite communications need to receive the signal is not only related to the frequency, but also related to the location, time, etc., coupled with the long transmission distance, resulting in transmission delay, which creates favorable conditions for interference [15]-[17]. In order to further improve the spectrum utilization and communication quality of satellite

communication, it is of great significance to study the detection of low-orbit satellite signal interference, and there are more algorithms for the detection of interfering signals at present, in which the main detection algorithms include the energy detection method, the cyclic smoothing analysis method, and so on, and with the development of artificial intelligence, the deep conviction network method based on deep learning algorithms is able to realize the automatic detection of signal interference[18]-[21].

Satellite communications, as an important part of the global communications infrastructure, play an irreplaceable role in the fields of national defense and military, emergency disaster relief, telemedicine and information transmission. In particular, low-orbit satellite communication system is becoming an important development direction of global communication network due to its advantages of low latency, high bandwidth and wide coverage. However, satellite communication systems are highly susceptible to various types of interference signals in complex electromagnetic environments, leading to degradation or even interruption of communication quality. These interferences may originate from the natural environment, man-made attacks or within the system, and their characteristics include diversity, complexity and uncertainty. In order to guarantee the reliable operation of LEO satellite communication system, the accurate detection and classification of interference signals become especially critical. Traditional interference detection methods mainly rely on techniques such as signal energy detection, matched filtering and statistical characterization, which are practical but difficult to accurately identify the type of interference in complex electromagnetic environments, especially the limited ability to detect unknown interference. In recent years, machine learning, especially deep learning technology, has shown strong potential in the field of signal processing, providing new ideas for automatic detection of interference signals. Deep belief network, as a deep learning model, excels in signal classification and anomaly detection by virtue of its powerful feature extraction and nonlinear mapping capabilities.

Based on the above background, this study proposes an automatic low orbit satellite signal interference detection method based on improved deep belief network. First, seven typical interference signal models are constructed to comprehensively cover the common types of interference in practical applications; Second, the interference signal characteristics are analyzed from both time and frequency domains to extract the feature parameters that can effectively distinguish different types of interference; then, to address the problems of slow convergence and low fine-tuning accuracy of the traditional deep belief network, the radial basis function is introduced as the activation function, and combined with the k-step contrastive scattering algorithm and adaptive moment estimation algorithm for improvement; Finally, the low orbit satellite signal interference detection process is designed to realize the accurate classification of known interference and the effective detection of unknown interference. The effectiveness of the proposed method is verified through simulation experiments, which provides theoretical support and technical guidance for the enhancement of anti-interference capability of LEO satellite communication system.

II. Satellite interference signal characterization

Satellite communication technology is the inheritance and development of terrestrial microwave relay communication and space technology, the use of communication satellites as a relay station to realize voice, data, multimedia and other communication services between mobile or fixed users on the ground end [22].

II. A.Modeling of interference signals

In this subsection, we will study seven typical interference signals in satellite communication systems: single-tone interference, multi-tone interference, narrowband noise interference, broadband noise interference, comb spectrum interference, broadband linear sweep interference, and impulse interference, and analyze their time-domain and frequency-domain characteristics.

(1) Single-tone interference

Single-tone interference refers to single-frequency continuous wave interference (CWI) in the communication frequency band, which generates interference at a specific frequency. Single-tone interference makes the satellite communication signal power amplification at a specific frequency point, while there is no effect on other frequency points, single-tone interference has the characteristics of simple structure, easy to realize, and concentrated interference energy, and the time-domain expression of single-tone interference is:

$$I(t) = \sqrt{2P_w}\cos\left(2\pi f_c t + \varphi\right) \tag{1}$$

where P_w is the power of the single-tone interference, f_c is the carrier frequency, and φ is the phase, uniformly distributed within $[0, 2\pi)$.

(2) Multi-tone interference

Multi-tone interference (SCWI) refers to the existence of single-frequency point interference at multiple random or fixed frequency locations in the communication band. Multi-tone interference is characterized by similar features as single-tone interference, with centralized capability and easy to implement. Its time domain expression is:

$$I(t)=\sum_{i=1}^{J}\sqrt{2P_w/J}\cos\left(2\pi f_{I,i}t+\varphi_i\right) \tag{2}$$

where $f_{I,i}$ is the i th carrier frequency of the multi-tone interference, J is the total number of frequency points, and φ_i is the phase corresponding to $f_{I,i}$, obeying a uniform distribution in $[0,2\pi)$.

(3) Narrowband noise interference

Narrowband noise interference (NBI) is relative to the full frequency band of communication interference band accounted for a relatively small noise interference, interference energy is relatively concentrated, if the carrier frequency of the communication signal jumps into the narrowband interference band range, the communication BER will greatly increase, seriously affecting the performance of communication. The generation of narrowband noise interference is relatively simple.

First generate random Gaussian white noise $n(t)$, which is the full frequency band noise, and then let $n(t)$ through the narrow-band filter $h(t)$, the window function $H(j2\pi f)$ for the impulse response after Fourier inversion $h(t)$, the time-domain expression of the narrow-band noise interference is:

$$I(t)=\int_{-\infty}^{+\infty}n(\tau)h(t-\tau)d\tau \tag{3}$$

$$H(j2\pi f)=\begin{cases}1, & |f\pm f_c|\le\dfrac{W_I}{2}\\ 0, & \text{Other}\end{cases} \tag{4}$$

where f_c is the center frequency of narrowband noise interference and W_I is the interference bandwidth. Narrowband noise interference bandwidth accounts for a small proportion of the total bandwidth of communication, if the center frequency of interference falls into the frequency band occupied by the communication signal, the communication signal can form a great threat.

(4) Wideband noise interference

Wideband noise interference (WBI) refers to the ability to communicate the whole frequency band or most of the frequency band for noise interference. Wideband noise interference in the case of the enemy does not know the relevant parameters of the communication, but also able to interfere with each other's communication band, and only need to set the power of the interference source is large enough, you can cause serious interference to the enemy's communications, so that the enemy's communication system quality is seriously degraded, but this produces a wideband noise interference power consumption cost is very large.

The Gaussian white noise $n(t)$ is generated first, and then $n(t)$ is allowed to pass through as a broadband filter $h(t)$, and then passes through an amplifier to obtain interference with larger energy. The broadband noise interference expression can also be expressed in equation (4), the difference is that its impulse response $h(t)$ is determined by according to the bandwidth of the communication signal, and the Fourier transform of $h(t)$, $H(j2\pi f)$, is expressed as:

$$H(j2\pi f)=\begin{cases}1, & |f|\le W_I\\ 0, & \text{Other}\end{cases} \tag{5}$$

(5) Comb Spectrum Interference

Comb Spectrum Interference (CSI) refers to the communication of multiple locations in the full frequency band for noise interference, combining the characteristics of narrow-band noise and wide-band interference, comb spectrum interference energy is relatively concentrated, and relatively easy to produce a more serious impact on the enemy in the case of unknown communication parameters.

Comb spectral interference is also generated by first generating a full-band random Gaussian white noise $n(t)$, and then passing through a filter with a time-domain impulse response of $h(t)$. The time-domain expression for comb spectral interference can also be expressed by Eq. (4), with the difference that the selection of the time-domain impulse response of $h(t)$ is based on the decision of the communication band to be interfered with, which

can be either continuously distributed or randomly distributed, with the impulse response $h(t)$ Fourier transform $H(j2\pi f)$ is given:

$$H(j2\pi f)=\begin{cases}1, & \left|f\pm f_{I,i}\right|\le\dfrac{W_{I,i}}{2}\\ 0, & \text{Other}\end{cases} \tag{6}$$

where the set of center frequencies of the comb spectrum interference bands is $\{f_{I,i}\}$, which is a collection of several consecutive or random frequency bands, and $\{W_{I,i}\}$ is the set of interference bandwidths corresponding to $\{f_{I,i}\}$.

(6) Broadband Linear Sweep Interference

Broadband linear frequency sweeping interference (LFMI) refers to the interference whose frequency varies linearly with time, and a higher sweeping rate is prone to form broadband interference, i.e., interference in most of the communication frequency bands. It is a dynamic non-stationary signal, whose frequency can change linearly with time periodically, and it interferes with the communication frequency band on a large scale, which seriously affects the communication performance.

The frequency of broadband linear sweep interference shows a wide band over a period of time and a single tone at a point in time, and its frequency varies linearly with time over a sweep period. Its time domain expression is shown in equation (7):

$$I(t)=A(t)\cos(\pi\mu_0 t^2+2\pi f_0 t+\varphi_0) \tag{7}$$

where the linear sweep signal time domain amplitude $A(t)=A\cdot rect(t/T)=\begin{cases}A, & 0\le t\le T\\ 0, & \text{Other}\end{cases}$, f_0 is the initial frequency, μ_0 is the sweep rate, φ_0 is the initial phase, and T is the sweep period.

(7) Pulse Interference

Pulse interference (PI) refers to the strong amplitude impulsive noise generated in a very short time, is a short-lived transient electromagnetic pulse, whose main characteristics are short duration, impulse amplitude, long time interval, discontinuous, irregular, sudden and strong. Impulse interference is often generated artificially, usually its impact on the quality of communication will be much larger than the impact of Gaussian white noise, especially in the requirements of high-quality communications, such as in voice calls, data transmission services. Impulse interference can be generated in various forms, here a single rectangular pulse is used to form, then its time domain expression can be:

$$I(t)=\begin{cases}A, & |t|\le\dfrac{\tau}{2}\\ 0, & \text{Other}\end{cases} \tag{8}$$

where A is the signal amplitude of the pulse interference and τ is the pulse interference duration.

II. B.Interference signal feature extraction

In the process of data analysis, the purpose of feature parameter extraction is to extract the parameter features with research value from the redundant and complex raw data, so as to reduce the time-consuming computation and improve the efficiency of signal recognition. In terms of parameter extraction, the main parameter features are obtained from two perspectives: time-domain features and frequency-domain features. Time-domain feature extraction is usually related to the amplitude of the signal, and it is not easy to express other features of the signal. Through some transformations from the time domain to the frequency domain, the distribution of the signal at each frequency can be visualized from the frequency domain to obtain richer signal features [23].

II. B. 1) 3dB bandwidth of normalized spectrum

Analyzing the above seven kinds of interference signals, it is not difficult to find that some signals have a relatively narrow spectral range, such as single-tone interference, multi-tone interference, etc., which are just impact points at certain frequency points, while some signals have a relatively wide spectral width, such as narrow-band noise interference (NBI) and wide-band noise interference (WBI). Thus based on the difference in the spectral width of the signal the signal can be categorized into wideband interference and narrowband interference. The above signals

can be distinguished by the 3dB bandwidth of the parameterized normalized spectrum. First define the normalized form of the signal:

$$\bar{P}_u(n) = \frac{P(n)}{E[P(n)]} \tag{9}$$

where $E[*]$ represents taking the mean value for *. where $P(n)$ represents the spectral value of the received interference signal. Let the normalized 3 dB bandwidth B_w of the interference be as follows:

$$B_w = \frac{m1 - m2 + 1}{N} \tag{10}$$

$$m1 = \max_{\bar{P}_u(n) > P_{th}} (n) \tag{11}$$

$$m2 = \min_{\bar{P}_u(n) > P_{th}} (n) \tag{12}$$

where $1 \le n \le N$. N denotes the number of frequency points where the interference signal is received. $P_{th} = 0.5 * \max[\bar{P}_u(n)]$. The variation of the normalized spectral 3dB bandwidths of the seven interfering signals with respect to the dry-to-noise ratio is shown in Fig. 1. It can be seen that the B_w values of both the single-tone interference (CWI) and the narrowband noise interference (NBI) signals are relatively small, while the B_w of the comb-spectrum interference (CSI), the pulsed interference (PI), and the wideband noise interference (WBI) are relatively large. The values of multi-tone interference (SCWI) and swept frequency interference (LFMI) are uncertain. It can also be seen that the value of B_w tends to be constant as the dry-to-noise ratio keeps increasing, and it can be seen that the noise affects the extraction of B_w eigenvalues differently for different interference signals. Therefore it can be realized that the B_w parameter can be used to classify and identify some signals.

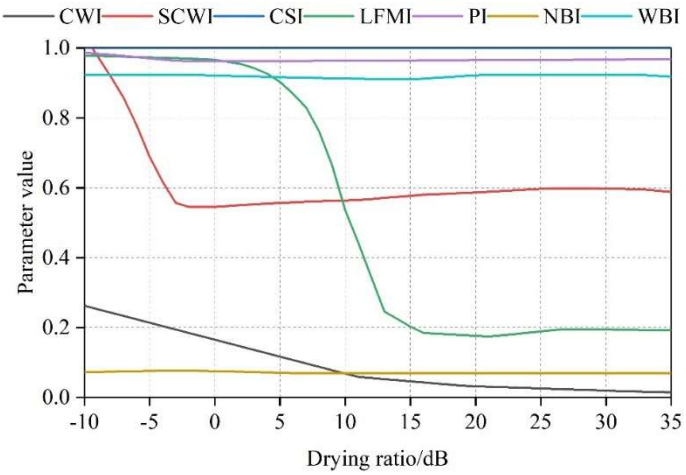

Figure 1: The variation of the bandwidth of the spectrum 3db with the noise ratio

II. B. 2) Peak-to-average ratio in the frequency domain

The frequency domain peak-to-average ratio parameters are defined as follows:

$$As = \frac{\max(P(n))}{mean(P(n)')} \tag{13}$$

where $\max(P(n))$ represents the maximum value in the signal spectrum. $mean(P(n)')$ represents the mean value of 30% of the signal spectrum in descending order. It represents the ratio of the peak of the signal spectrum to the mean value of the larger portion of the signal amplitude.

The variation of the frequency domain peak-to-average ratio As with JNR as shown in Fig. 2 shows that the parameter gradually stabilizes as the dry noise ratio continues to increase. Among them, the parameter of single-tone interference gradually increases, the value of As of multi-tone interference (SCWI) is close to 5, and the

values of the parameters of the remaining five types of interfering signals are almost close to 1-3. Therefore, the classification of single-tone interference can be realized by setting appropriate threshold values.

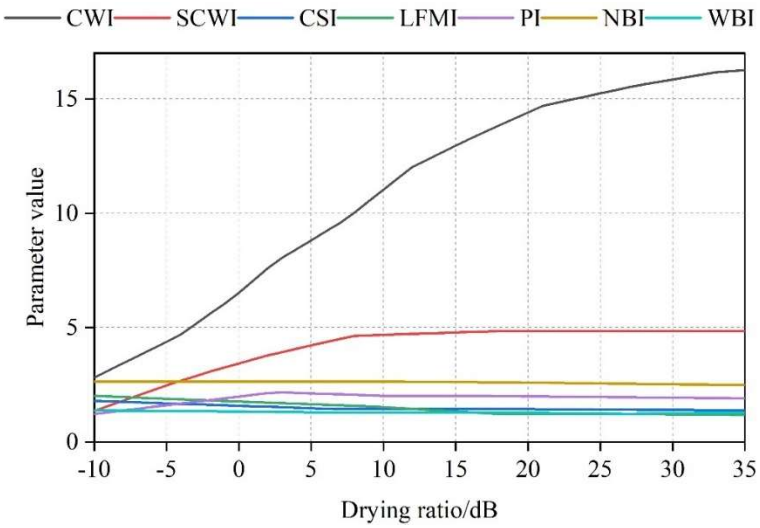

Figure 2: The frequency range peak is compared to the change of As with the JNR

II. B. 3) Moment Bias in the Frequency Domain

Analogous to the time domain moment skewness of a signal, the frequency domain moment skewness is expressed as:

$$b3 = \frac{E(P(n)-\mu)^3}{\sigma^3} \tag{14}$$

The frequency domain moment skewness responds to the degree of deviation of the signal spectrum relative to the central distribution. The characteristic curves of $b3$ for seven signals with different dry-to-noise ratios are shown in Fig. 3. From the figure, it can be seen that the value of the frequency domain moment skewness $b3$ for the single-tone interference (CWI) is close to 15, the frequency domain moment skewness $b3$ for the multi-tone interference (SCWI) is close to 8, where the frequency domain moment skewness $b3$ for the narrow-band noise interference (NBI) and the pulsed interference (PI) is relatively close to 4, and that for the swept-frequency interference (LFMI) is close to 3, and the rest of the comb spectral interference (CSI) and wide-band noise interference (CSI) are close to 4, and the remaining comb spectral interference (CSI) and wide-band noise interference (CSI) are close to 3. CSI) and Wideband Noise Interference (WBI) have the same frequency domain moment skewness $b3$ value close to 1. Thus, the interfering signals can be categorized by appropriate threshold values.

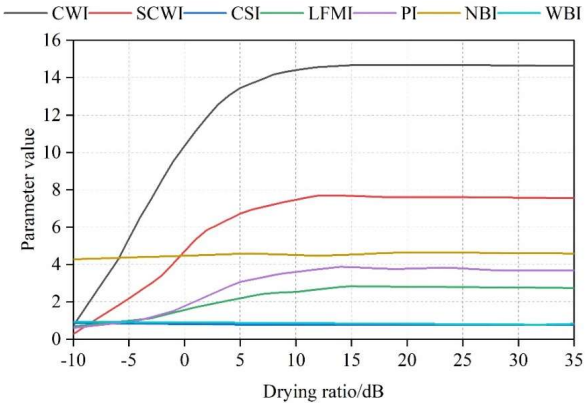

Figure 3: The frequency domain moment deviation $b3$ is changing with the JNR

III. DBN-based automatic detection model for low-orbit satellite signal interference

III. A. Restricted Boltzmann machines

The Restricted Boltzmann Machine (RBM) is the basic unit of a deep belief network [24], and its model structure is shown in Fig. 4. The model consists of implicit and visible layers, with bidirectional full connectivity between layers and no connectivity within layers.

In Fig. 4 W is the weight matrix connecting the visible layer to the hidden layer. n and m are the number of neurons in the hidden and visible layers, respectively. $v=[v_1,v_2,\cdots,v_m]^T$ is the state vector of the visible layer. $h=[h_1,h_2,\cdots,h_n]^T$ is the state vector of the hidden layer. $a=[a_1,a_2,\cdots,a_m]^T$ is the bias vector of the visible layer. $b=[b_1,b_2,\cdots,b_n]^T$ is the bias vector of the implicit layer.

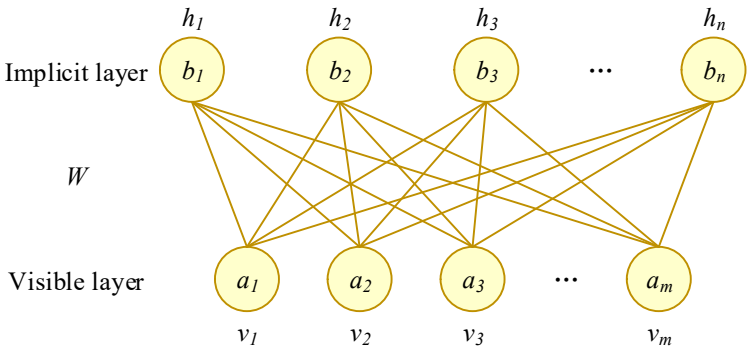

Figure 4: Restricted Boltzmann machine

The energy function of the joint RBM Bernoulli (visible layer)-Bernoulli (hidden layer) state can be expressed as:

$$E(v,h)=-\sum_{i=1}^{m}a_i v_i-\sum_{j=1}^{n}b_j h_j-\sum_{i=1}^{m}\sum_{j=1}^{n}w_{ij}v_i h_j \tag{15}$$

where, w_{ij} is the connection weight of RBM. The joint probability distribution function of the visible and hidden layers can be obtained by $E(v,h)$ as:

$$P(v,h)=\frac{e^{-E(v,h)}}{Z} \tag{16}$$

$$Z(\theta)=\sum_{v,h}e^{-E(v,h)} \tag{17}$$

where, $Z(\theta)$ is the normalization factor or the collocation function, which represents the (energy index) summation over all possible states of the set of nodes in the visible and hidden layers.

The joint probability distribution function $P(v,h)$ is known to yield an independent distribution for the visible layer as:

$$P(v)=\frac{1}{Z}\sum_{h}e^{-E(v,h)} \tag{18}$$

Due to the special fully connected between layers and unconnected within layer structure of the RBM model, the conditional probability distribution can be expressed as:

$$P(h_j=1/v)=\sigma\left(b_j+\sum_{i=1}^{m}v_i w_{ij}\right) \tag{19}$$

$$P(v_i=1/h)=\sigma\left(a_i+\sum_{j=1}^{n}w_{ij}h_j\right) \tag{20}$$

where, $\sigma(\cdot)$ is the activation function.

III. B. Improved Deep Belief Network Algorithm

Deep Belief Network (DBN) is a probabilistic generative model stacked with multiple Restricted Boltzmann Machines (RBMs), which is one of the main current implementations of deep learning.The DBN structural model is shown in Fig. 5.The DBN generally consists of multiple layers of stacked Restricted Boltzmann Machines (RBMs) as well as Soft-Max classifiers at the top layer. The input layer and the second layer form the first Restricted Boltzmann Machine structure, i.e., RBM1, and the second layer and the third layer form the second Restricted Boltzmann Machine structure, i.e., RBM2, and at the same time, the implicit layer of the upper layer is used as the visible layer of the next layer, and so on, which ultimately constitutes the structure of l RBMs. Then the output of the topmost layer is used as the input to the classifier, and the data is classified one by one based on the results of the classifier.The learning process of DBN is divided into two stages, i.e., unsupervised layer-by-layer pre-training of the RBMs and supervised backward fine-tuning of the whole network using the BP propagation algorithm.

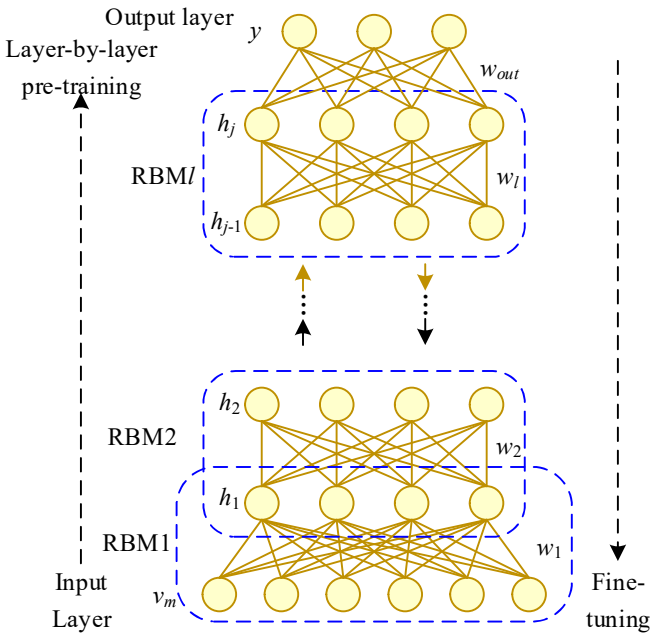

Figure 5 Structural model of DBN

Due to the problems of long convergence time of network model, low accuracy of backward fine-tuning, and poor adaptability to complex data distribution in the traditional DBN model, this paper proposes an improved DBN model: firstly, the radial basis (RBF) function is introduced as the activation function of the DBN, which improves the adaptability of the DBN model to complex data distribution. Second, the k -step contrast-dispersion (CD)- k algorithm is used for fast training in the unsupervised training phase of the RBM, and the adaptive moment estimation (ADAM) algorithm is used instead of the gradient descent algorithm for fine-tuning in the supervised training phase to improve the diagnostic accuracy of the DBN.

(1) Radial basis activation function model

The radial basis function is a monotonic function with the distance between the data $\mathbf{x}$ to a certain vector $\mathbf{c}$ as the independent variable, which is used as the activation function of the DBN, and the energy function can be expressed as:

$$E(v,h)=\sum_{i=1}^{m}\frac{(v_i-k_i)^2}{2\beta_i^2}-\sum_{j=1}^{n}\frac{(h_j-k_j)}{2\beta_j^2}-\sum_{i=1}^{m}\sum_{j=1}^{n}\frac{v_i h_j w_{ij}}{\beta_i\beta_j} \tag{21}$$

where, v_i is the value of the i th node in the visible layer, h_j is the value of the j th node1 in the hidden layer, w_{ij} is the value of the connection weights, β is the neuron width, and k is the neuron center point. The conditional probability distribution of the improved DBN can be expressed as:

$$P(h_j = 1/v) = \exp\left(\frac{-\left\|\sum_i v_i w_{ij} - k_j\right\|}{\beta_j^2}\right) \tag{22}$$

$$P(v_i = 1/h) = \exp\left(\frac{-\left\|\sum_j h_j w_{ji} - k_i\right\|}{\beta_i^2}\right) \tag{23}$$

(2) Unsupervised pre-training phase

The unsupervised pre-training phase of DBN refers to updating the network parameters $\theta = \{w_{ij}, a_i, b_j\}$ by training each RBM layer-by-layer, in order to reduce the pre-training duration, the normalization factor $Z(\theta)$ in Eq. (17) is required to be calculated. Since it is difficult to compute it by the plain method, this paper adopts the $CD-k$ algorithm for fast unsupervised training of the pre-training process. The core of the $CD-k$ algorithm is Gibbs sampling, which uses the K-L distance between the estimated probability distribution and the true probability distribution as a metric criterion to Gibbs sample the training samples to generate samples with maximum probability.

By calculating the gradient of the log-likelihood formula $\log P(v)$, the RBM weight update formula is obtained as:

$$\begin{cases} \Delta w_{ij} = \mu(\langle v_i h_j \rangle_{data} - \langle v_i h_j \rangle_{recon}) \\ \Delta a_i = \mu(\langle v_i \rangle_{data} - \langle v_i \rangle_{recon}) \\ \Delta b_j = \mu(\langle h_j \rangle_{data} - \langle h_j \rangle_{recon}) \end{cases} \tag{24}$$

where, μ is the learning rate, $data$ and $recon$ denote the probability distribution of the training data and the reconstructed probability distribution, respectively. According to the Markov chain principle, the above weight update problem is converted into an unbiased model, which can be achieved when Gibbs sampling is long enough.

(3) Supervised backward fine-tuning stage

The reverse fine-tuning stage is the supervised training carried out after completing the pre-training, which serves to fine-tune the relevant parameters of the DBN model and reduce the error between the model output and the actual labels, so as to achieve the optimization of the overall DBN model. In order to improve the diagnostic accuracy of the DBN model, this paper adopts the ADAM algorithm instead of the traditional gradient descent algorithm, which dynamically adjusts the learning rate by utilizing the first-order moment estimation and the second-order moment estimation of the gradient to provide a smoother and more stable parameter gradient for updating the weight parameters. In unsupervised pre-training, the network parameters $\theta = \{w_{ij}, a_i, b_j\}$ are obtained after k iterations, and the first-order moment estimation m_{k+1} and the second-order moment estimation v_{k+1} are updated by calculating $g = \nabla J(\theta_k)$ as:

$$\begin{cases} m_{k+1} = \beta_1 m_k + (1-\beta_1) g \\ v_{k+1} = \beta_2 v_k + (1-\beta_2) g^2 \end{cases} \tag{25}$$

The first-order moment deviation $\hat{m}_{k+1}$ and the second-order moment deviation $\hat{v}_{k+1}$ are:

$$\begin{cases} \hat{m}_{k+1} = m_{k+1} / (1-\beta_1^{k+1}) \\ \hat{v}_{k+1} = v_{k+1} / (1-\beta_2^{k+1}) \end{cases} \tag{26}$$

The updated network parameter θ_{k+1} is:

$$\theta_{k+1} = \theta_k - \alpha \hat{m}_{k+1} / \left(\sqrt{\hat{v}_{k+1}} + \tau\right) \tag{27}$$

where, α is the step size, β_i is the decay rate, and τ is the stabilization constant.

III. C. Low-orbit satellite signal interference detection process

For LEO satellites, the traditional state χ^2 detection method can detect whether the signal is interfered or not, but cannot recognize the type of interference. Therefore, this paper proposes an interference signal detection algorithm with improved DBN, which utilizes the improved DBN for interference detection on the basis of the state χ^2

detection method for satellites to achieve accurate identification, localization and isolation of interference signals, and to improve the stability of the low-orbit satellite signals, and its specific structure is shown in Figure 6.

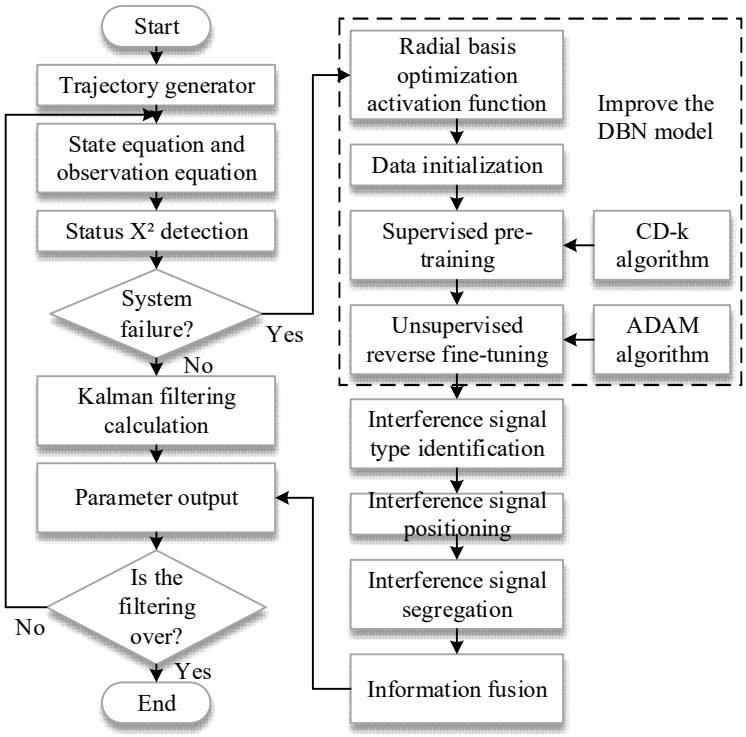

Figure 6: The detection process of the interference signal based on improved DBN

IV. Performance evaluation of automated low orbit satellite signal interference detection

IV. A. Experimental environment and evaluation indicators

The simulation environment for this experiment is GPU, and the deep learning framework PyTorch is used for the training and testing of the convolutional neural network. The network is initialized with random initialization for the weight parameters, the learning rate is set to 0.002, and the batch size is 68.In the experiment, the simulation software MATLAB is used to generate simulated communication interference signals, and the simulated communication interference signals include single-tone interference (CWI), multi-tone interference (SCWI), narrow-band noise interference (NBI), and wide-band noise interference (WBI), Comb Spectrum Interference (CSI), Wideband Linear Frequency Sweep Interference (LFMI), and Pulse Interference (PI), the seven kinds of communication interference signals, the channel noise is additive Gaussian white noise, and the range of the dry-to-noise ratio is from -6dB to 13dB, and 2,000 samples are generated by simulation of each interference signal at each dB, of which 1,300 samples are used as the training set, 350 samples are used as the validation set, and 350 samples are used as the test set.

In the experimental process, seven kinds of interference signals are respectively used as unknown signals for seven experiments, and the recognition and detection results are obtained when seven kinds of signals are respectively used as unknown signals. The following is a detailed description of the experimental process using comb spectrum interference as an unknown interference signal as an example.

Use the training set to train the network, then use the trained network to identify the interference signal in the validation set, count the distribution of the confidence scores of the correctly classified interference signal on the validation set, set the threshold according to the distribution and the actual demand, and finally use the threshold and the trained network to determine whether the signal in the test set is a known interference or an unknown interference.

Considering the unknown interference signal as 1 and the known signal as 0, the confusion matrix established is shown in Table 1. Where TP is the number of unknown disturbances detected as unknown disturbances, FP is the number of known disturbances detected as unknown disturbances, FN is the number of unknown disturbances detected as known disturbances, and TN is the number of known disturbances detected as known disturbances. Therefore, the detection probability TPR for unknown interference and the false alarm probability FPR for detecting

known interference as unknown interference can be obtained from this, and their specific expressions are shown in Eqs. (28) and (29):

$$TPR = \frac{TP}{TP + FN} \tag{28}$$

$$FPR = \frac{FP}{FP + TN} \tag{29}$$

Table 1: Confusion matrix

		Real category	
		1	0
Detection category	1	TP	FP
	0	FN	TN

For the above confusion matrix, a plurality of TPRs and FPRs can be obtained by setting different thresholds, and by using these FPRs as the horizontal coordinates and TPRs as the vertical coordinates, the ROC curve graph of the present method can be obtained. The horizontal and vertical coordinates of the points on the curve represent the false alarm probability and the detection probability of the detection of the unknown signal by the present method obtained when the threshold is fixed to a certain value, respectively. The area enclosed by the ROC curve and the horizontal axis is denoted as AUC, and it is easy to know that the size of AUC should be between 0 and 1. The demand in practical applications is generally the higher the detection rate of unknown signals, the better, the lower the false alarm rate, the better, reflected in the ROC curve is the upper left point, the ROC curve composed of such points corresponds to the AUC is also larger, so generally speaking, the larger the value of the AUC, the better the detection effect of the model. Therefore, in this experiment, the AUC is used as the evaluation standard for the detection effect of unknown interference.

IV. B. Experimental results and analysis

In the experiment, the distribution of the confidence score c over the correctly classified interfering signals on the validation set was obtained, as shown in Fig. 7. The threshold T is set to 0.7 in this experiment. i.e., for c greater than T in the test set, the output is the signal type recognized by the classification branch. For c less than T, the output is the unknown signal type.

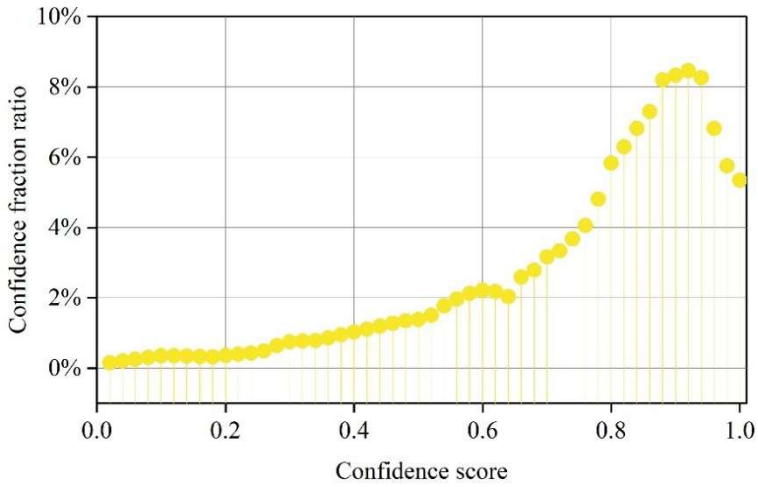

Figure 7: The confidence score is distributed on the validation set

The interference signals in the test set were passed through the trained network and the confidence scores of all the known and unknown interferences on the test set were obtained and their distribution is shown in Fig. 8. The distribution of the confidence scores on the test set shows that there is some overlap in the values of the confidence scores of the known and unknown signals, but most of them have been distinguished. After passing through the trained network, the confidence scores obtained for the known disturbances are mostly greater than 0.7, and the

distributions of the unknown signals are mostly less than 0.7. Moreover, it is found that the distributions of the confidence scores of the validation set and the test set on the known disturbances signals are similar, so that the method of using the validation set for determining the threshold value T is reasonable and effective.

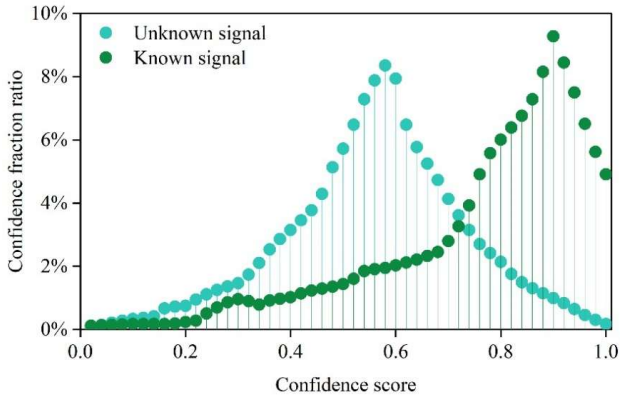

Figure 8: The confidence score is distributed on the test set

With the threshold T set to 0.7 in this experiment, the false alarm probability of known interference detection as unknown interference is 0.3, and the probability of detection for unknown signals is 0.8. In addition, one can achieve one's desired detection effect by appropriately adjusting the size of the threshold T according to the distribution of confidence scores on the validation set based on the sensitivity of the experimental project to unknown signals. Also the corresponding ROC curve of Fig. 7 is shown in Fig. 9, and its corresponding AUC value is 0.825.

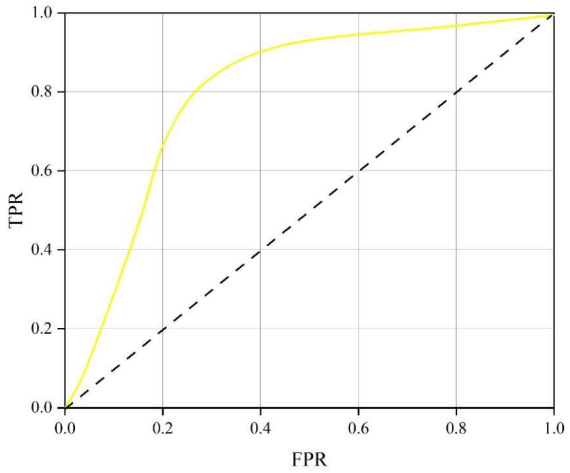

Figure 9: The comb interference is a ROC graph of the unknown signal

Repeat the above steps, the unknown signal from the comb spectrum interference in turn for single-tone, multi-tone, narrow-band, swept signal respectively for the above experiments, and ultimately get the detection of seven kinds of interference signals respectively as the unknown interference signal when the detection of the identification, each interference as an unknown signal when the detection of the ROC curve is shown in Figure 10. For the interference signal identification model designed in this section by adding confidence scores, for these seven types of interference, the model has a certain unknown interference detection capability when each interference signal is treated as an unknown interference. The detection effect of the model is close for different interferences as unknown interferences, among which the model has the best unknown interference detection effect when comb spectrum interference is used as unknown interference.

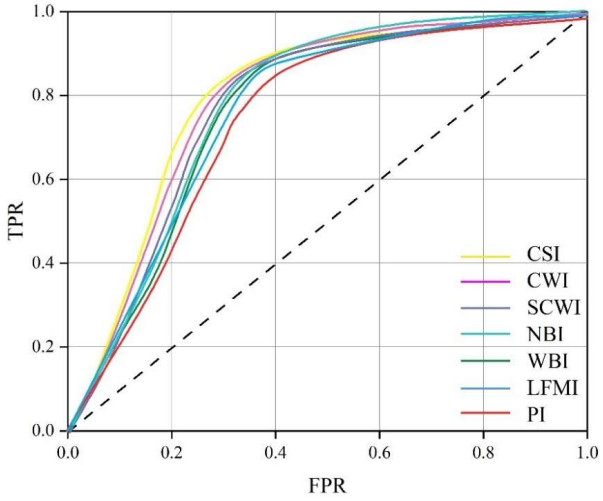

Figure 10: The various distractions are the ROC graphs of the unknown interference

The AUC values of each interference as unknown signals respectively are shown in Fig. 11. The AUC values are all above 0.7, among which, the comb spectral interference (CSI) has the highest AUC value of 0.806. It is verified that the deep belief network is the most effective in detecting the comb spectral interference signals.

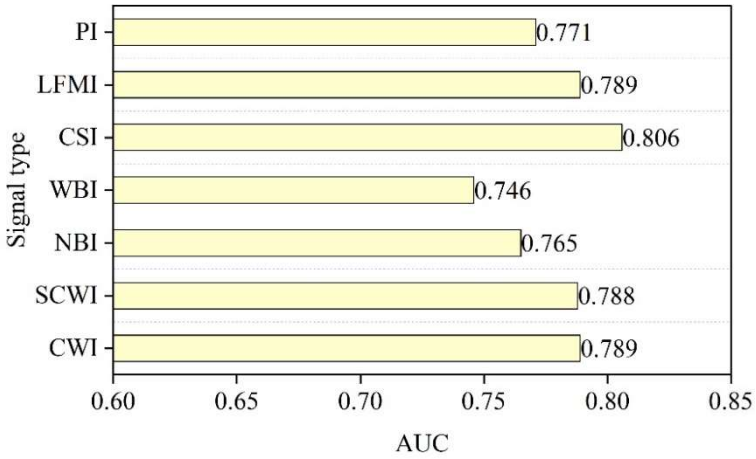

Figure 11: Unknown signal recognition performance

In summary, this paper investigates the interference signal recognition model that can detect unknown interference signals based on deep belief networks. The AUC values of each interference signal as an unknown signal respectively are above 0.7, and the model detects better and can accurately recognize several interference signals studied in the paper.

V. Conclusion

The following main conclusions have been obtained from the study of the automatic detection method of low-orbit satellite signal interference based on improved deep belief network:

The improved deep belief network model significantly improves the detection accuracy and identification efficiency of interference signals by introducing the radial basis function as the activation function, combined with the -step contrast-dispersion (CD)- algorithm and adaptive moment estimation algorithm. The experimental results show that, in the test environment with the dry-to-noise ratio ranging from -6dB to 13dB, the method performs well in the identification of seven typical interference signals, especially in the identification of comb-spectrum interference, with an AUC value of 0.825. When the threshold is set to 0.7, the detection probability of the proposed method on the test set for unknown interference is 0.8, and the false-alarm probability is controlled to be within 0.3, which verifies that the method can detect the unknown interference in the test set within 0.8. , verifying the effectiveness of the method in unknown interference detection. Through the frequency domain feature analysis, it is found that

the three feature parameters of normalized spectrum 3dB bandwidth, frequency domain peak-to-average ratio and frequency domain moment skewness have a better differentiation between different interference signals, which provides an effective way for the feature extraction of interference signals. The research results provide theoretical basis and technical support for the anti-interference design of low-orbit satellite communication system, which is of great value for improving the quality and reliability of satellite communication.

References

[1] Reznik, S. V., Reut, D. V., & Shustilova, M. S. (2020, November). Comparison of geostationary and low-orbit “round dance” satellite communication systems. In IOP Conference Series: Materials Science and Engineering (Vol. 971, No. 5, p. 052045). IOP Publishing.

[2] Liu, C., & Wu, Y. (2024, October). History and trends in the development of low-orbit satellite communication systems. In 2024 IEEE 24th International Conference on Communication Technology (ICCT) (pp. 1044-1048). IEEE.

[3] Lagunas, E., Chatzinotas, S., & Ottersten, B. (2024). Low-Earth orbit satellite constellations for global communication network connectivity. Nature Reviews Electrical Engineering, 1(10), 656-665.

[4] Sun, T., Hu, M., & Yun, C. (2022). Low-Orbit Large-Scale Communication Satellite Constellation Configuration Performance Assessment. International Journal of Aerospace Engineering, 2022(1), 4918912.

[5] Shen, H., Li, J., & Wang, Z. (2024). Design and Simulation of Low-Orbit Satellite Broadcast Signal Receiving and Processing Terminal. Electronics, 13(16), 3270.

[6] Hui, L. Z., & Yang, G. Q. (2018, December). Uplink user power control for low-orbit satellite communication systems. In 2018 IEEE 4th International Conference on Computer and Communications (ICCC) (pp. 634-639). IEEE.

[7] Shao, R., Fang, Z., Gao, S., Liu, S., Wang, Z., Nie, Y., & Xie, S. (2019). G-BDP-ADC model for effectiveness evaluation of low orbit satellite communication system in the context of poor information. IEEE Access, 7, 157489-157505.

[8] PASHINTSEV, V. P., PESKOV, M. V., KALMYKOV, I. A., ZHUK, A. P., & TOISKIN, V. E. (2020). METHOD FOR FORECASTING OF INTERFERENCE IMMUNITY OF LOW FREQUENCY SATELLITE COMMUNICATION SYSTEMS. AD ALTA: Journal of Interdisciplinary Research, 10(1).

[9] Liu, W., Cai, W., Liu, L., Wang, D., Lin, W., Wang, K., ... & Hu, J. (2024). A high-efficiency frequency synchronization scheme for low Earth orbit satellite communications based on dynamic game theory. International Journal of Satellite Communications and Networking, 42(2), 97-122.

[10] Anteur, M., Thomas, N., Deslandes, V., & Beylot, A. L. (2019). On the performance of UNB for machine-to-machine low earth orbit (LEO) satellite communications. International Journal of Satellite Communications and Networking, 37(1), 56-71.

[11] Shen, J., Liu, H., Wang, J., & Jia, X. (2021). Algorithm for frequency capture and rectification in a low-orbit satellite IoT communication network. Mathematical Biosciences and Engineering, 18(6), 7999-8023.

[12] Ondyrbayev, N., Zhumagali, S., Chezhimbayeva, K., Zhumanov, Y., & Nurzhauov, N. (2024). Development and Research of an Autonomous Device for Sending a Distress Signal Based on a Low-Orbit Satellite Communication System. Journal of Applied Data Sciences, 5(3), 1258-1271.

[13] Torrens, S. A., Petrov, V., & Jornet, J. M. (2024). Modeling interference from millimeter wave and terahertz bands cross-links in low earth orbit satellite networks for 6G and beyond. IEEE Journal on Selected Areas in Communications, 42(5), 1371-1386.

[14] Hao, C., Feng, D., Zhang, Q., & Xia, X. G. (2020). Interference geolocation in satellite communications systems: An overview. IEEE Vehicular Technology Magazine, 16(1), 66-74.

[15] Qiao, J., Lu, Z., Lin, B., Song, J., Xiao, Z., Wang, Z., & Li, B. (2023). A survey of GNSS interference monitoring technologies. Frontiers in Physics, 11, 1133316.

[16] Zheng, J., Xu, F., Zhu, Y., Lv, J. Z. Q., Guo, R., & Chen, Y. (2025). Low-orbit satellite signal interference detection based on fast regional convolutional network and its multidimensional evaluation method. J. COMBIN. MATH. COMBIN. COMPUT, 124(501), 512.

[17] Stock, W., Schwarz, R. T., Hofmann, C. A., & Knopp, A. (2024). Survey on opportunistic PNT with signals from LEO communication satellites. IEEE Communications Surveys & Tutorials.

[18] Tang, C., Zhou, X., Zhang, L., Liu, Y., & Dan, Z. (2025). LEO Satellite Navigation Signal Multi-Dimensional Interference Optimisation Method Based on Hybrid Game Theory. Remote Sensing, 17(8), 1444.

[19] Qing-yang, G., & Wu, S. (2021). Signal Detection in Satellite-Ground IoT Link Based on Blind Neural Network. Wireless Communications & Mobile Computing (Online), 2021.

[20] Zheng, J., Lv, Q., Xu, F., Zhu, Y., Zhou, J., Guo, R., & Chen, Y. (2025). Study on collaborative spectrum sensing of multi-satellite low orbit satellites based on multi-satellite collaborative beamforming and intelligent algorithms. J. COMBIN. MATH. COMBIN. COMPUT, 127, 7611-7627.

[21] Meng, S., Jia, M., Guo, Q., & Gu, X. (2021, July). Inter satellite link interference detection and analysis of NGSO satellite system. In International Conference on Wireless and Satellite Systems (pp. 1-11). Cham: Springer International Publishing.

[22] JinLiu,XiangruWang,FengLiang & ChundiWu. (2024). 61-2: Implementation of Phased Array Antennas Based on Liquid Crystal Technology in Simulated Satellite Communication Systems. SID Symposium Digest of Technical Papers,55(S1),524-526.

[23] Vikas Malhotra,Gurpreet Singh Saini,Sumit Malhotra & Renu Popli. (2024). Design of a robot system for improved stress classification using time–frequency domain feature extraction based on electrocardiogram. Paladyn,15(1),

[24] Jin Hong Kim,Hyun Wook Kim,Min Jung Chung,Dong Hoon Shin,Yeong Rok Kim,Jaehyun Kim... & Cheol Seong Hwang. (2024). A stochastic photo-responsive memristive neuron for an in-sensor visual system based on a restricted Boltzmann machine. Nanoscale horizons,